

# MRI only radiotherapy planning using the transfer function estimation algorithm

Rickard O. Cronholm<sup>1</sup>, Anders Karlsson<sup>1</sup>, Carl Siversson<sup>1,2\*</sup>

## Abstract

In order to enable an MRI-only workflow in radiotherapy treatment planning, methods are required for generating Hounsfield unit maps (i.e. synthetic CT, sCT) for dose calculations and patient positioning, directly from MRI. The transfer function estimation (TFE) algorithm is a method for automatically generating sCT images from a single MR acquisition sequence, based on a deep convolutional neural network and a spatially variant affine transfer function. This study compares dose calculations and patient positioning between sCT generated by the TFE algorithm and conventional CT in the male pelvic region.

The study comprised images for 34 prostate cancer patients acquired at four separate radiotherapy centers. For each patient, a multi-slice T2 weighted MRI and a conventional planning CT were acquired. Synthetic CT images were generated from the acquired MRIs using the TFE algorithm. In order to decouple the effect of variations in patient geometry between imaging modalities from the effect of any uncertainties in the TFE algorithm, the MRI was non-rigidly registered to the CT prior to generating the sCT. For each patient, an Intensity Modulated Radiation Therapy (IMRT) plan was created based on CT, and recalculated on sCT. In addition, for a subset of patients, the CT and the sCT were rigidly registered to a cone beam CT (CBCT) acquired for patient positioning prior to treatment delivery.

The difference between CT and sCT were evaluated using several methods. Mean absolute error (MAE) within the body contour was  $39.6 \pm 6.7$  HU. Average mean absorbed dose difference to target was  $-0.02 \pm 0.30\%$ . The average gamma pass rate (2% dose/2mm) was 99.9%. Average patient positioning verification difference was  $0.02 \pm 0.27$  mm and  $0.05 \pm 0.29^\circ$ . All uncertainties are given as one standard deviation of the population.

In total, the TFE algorithm enables a highly accurate MRI only workflow in prostate radiotherapy planning. Any uncertainties originating from the TFE algorithm, concerning dose accuracy or patient positioning verification, appear negligible.

<sup>1</sup>Spectronic Medical AB, Helsingborg, Sweden

<sup>2</sup>Department of Medical Radiation Physics, Lund University, Malmö, Sweden

\*Corresponding author: carl.siversson@spectronic.se

Published: June 2020

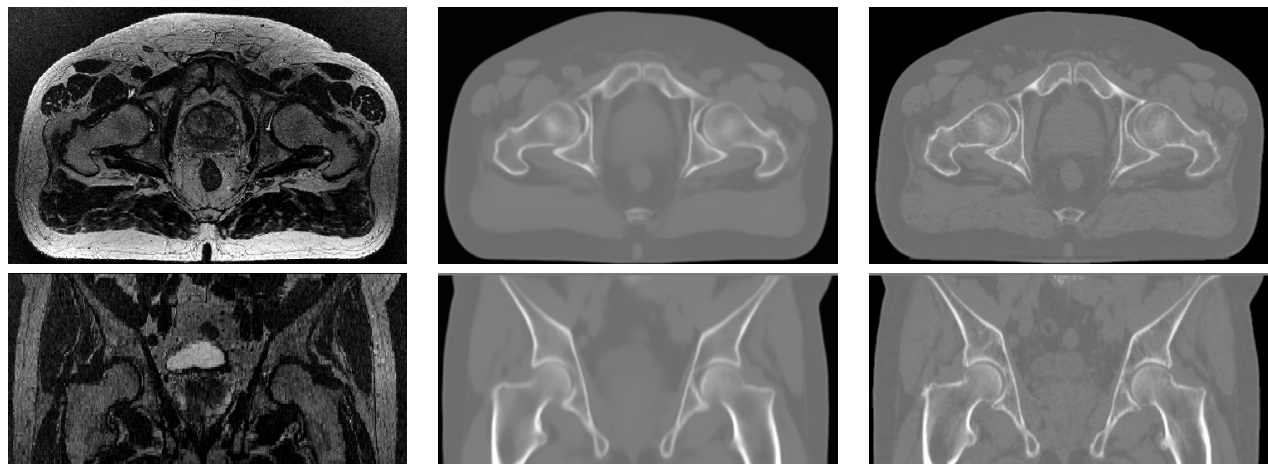


Image examples for a typical prostate case. To the left is a T2 weighted multi-slice MRI, in the middle the generated synthetic CT and to the right is the corresponding conventional CT. The top row shows slices in the anterior plane, while the bottom row shows slices in the coronal plane.

## Contents

<b>1</b>	<b>Introduction</b>	<b>2</b>
<b>2</b>	<b>Methods</b>	<b>2</b>
2.A	Image acquisition . . . . .	2
2.B	Image registration . . . . .	2
2.C	Synthetic CT generation . . . . .	3
2.D	Treatment planning . . . . .	3
2.E	Patient positioning verification . . . . .	4
2.F	Evaluation . . . . .	4
<b>3</b>	<b>Results</b>	<b>5</b>
<b>4</b>	<b>Discussion</b>	<b>5</b>
<b>5</b>	<b>Conclusions</b>	<b>6</b>
	<b>Acknowledgments</b>	<b>6</b>
	<b>References</b>	<b>6</b>

## 1. Introduction

The limited soft tissue contrast of computed tomography (CT) often makes accurate target and risk organ delineation for radiotherapy difficult. In several publications it has been shown that the addition of magnetic resonance imaging (MRI) guidance adds substantial value to the delineation process[1, 2]. The clinical benefit of such multimodal imaging has motivated a rapidly increasing usage of MRI in clinical practice. However, there are several disadvantages associated with the use of multiple imaging modalities, including the increased costs and the additional geometrical uncertainties introduced by the multiple imaging sessions. Such uncertainties include both inaccuracies when repositioning the patient between imaging sessions, as well as any errors in the registration of the acquired MR and CT images. For these reasons, it has been suggested that an MRI only workflow would be beneficial to the radiotherapy planning process, both in terms of costs and accuracy, since the disadvantages of a multimodal imaging workflow would then be avoided[3].

Since MRI does not directly provide the physical properties of the tissue expressed in Hounsfield units (HUs) as required for dose calculation, methods are required for synthetically generating this information (i.e. synthetic CT, sCT) based on MRI data. Several attempts at finding a solution to this problem have been presented. One suggested approach is to approximate the CT value in a voxel, based on a transform which utilizes corresponding voxel values from a combination of MRIs, acquired using different pulse sequences[4, 5, 6]. A disadvantage with this type of methods is that non-standard pulse sequences are typically required and that even subtle patient movement between the acquisition of these sequences may generate an HU error. Another suggested approach is to approximate a synthetic CT image by deforming a model or a set of reference CT images to match a new patient MRI[7, 8]. The obstacle to overcome with such methods is how to manage patients with atypical anatomy, since the deformation process might not be optimal under such circumstances. A

third approach is to utilize a convolutional neural network to perform the conversion from MRI to sCT[9]. A challenge with this method is that the quality of the generated sCT is highly dependent on the accuracy by which the MRI and CT training datasets are aligned. Such method is also limited to processing images resampled to the same resolution as was used during training.

In order to allow for widespread clinical adoption of an MRI only workflow in radiotherapy planning, the above-mentioned limitations need to be resolved, such that reliable sCT images can be generated with minimal effort also in a routine clinical environment with any MRI scanner equipped for use in radiotherapy. The transfer function estimation (TFE) algorithm is a recently developed commercial method, designed to achieve this goal. The TFE algorithm automatically generates sCT images from a single standard MRI acquisition, based on a deep convolutional neural network and a spatially variant transfer function. The aim of this study is to evaluate sCT images generated using the TFE algorithm by comparing dosimetric accuracy, as well as Hounsfield unit variation and patient positioning accuracy, between sCT and conventional CT for a set of prostate cancer patients.

## 2. Methods

### 2.A Image acquisition

Analysis was retrospectively performed on data from 34 prostate cancer patients acquired at four Swedish radiotherapy centers. Images were acquired using 3T GE Discovery, 3T GE Signa, 1.5T Siemens Aera and 3T Siemens Skyra MRI scanners. Imaging was performed as part of a previous non-interventional multicenter study[10]. Inclusion criteria were patients referred to MR and CT imaging before prostate radiation therapy.

For each patient, a T2-weighted MR image with large field of view (FOV) was acquired, covering the entire patient contour, with sufficient coverage for treatment planning in the cranio-caudal direction (scan time around 5 minutes). Such sequence was added to the standard protocol consisting of target and marker localization sequences. All centers imaged the patients in treatment position on both CT and MR, using a flat tabletop and immobilization with ankle and knee support. In order to minimize geometrical distortion in the MRI, all images were acquired with a high acquisition bandwidth and with vendor specific distortion correction activated.

Magnetic resonance and CT imaging parameters are specified in table 1. The RF (radiofrequency) coils were centered over the symphysis on a stiff coil bridge. Quality assurance of the MR scanners was performed according to local practice at each center.

### 2.B Image registration

Since patients were repositioned between MRI and CT imaging, a slight divergence in tissue and organ positioning, as well as bladder and rectal filling, was inevitable between imaging

**Table 1.** Scan protocol parameters applied for the T2-weighted MR used for sCT generation and the CT.

Parameter	MRI	CT
Slice thickness [mm]	2.5–3.0	2.5–3.0
In-plane resolution [mm <sup>2</sup> ]	0.44–0.88×0.44–0.88	1.0×1.0
Voltage [kV]		120
Slice gap [mm]	0	0
Distortion correction	On	
Bandwidth [Hz/pixel]	244–390 @ 3T 215 @ 1.5T	
FOV [mm]	448	
# slices	88–100	
TE [ms]	96–98	
TR [ms]	11930–15000	
Flip angle [°]	130–160	
Acquisition type	2D	Multislice
Post processing	Homogenization	
Sequence type	Spin echo	

sessions. For this reason, there will always be an inherent variation between a CT and a generated sCT, which is not related to the quality of the sCT but instead to the repeatability by which a patient can be positioned. In order to minimize the effect of such inherent variations, each MRI was registered to its corresponding CT using a constrained non-rigid registration procedure. For such registration a modified version of the Elastix registration toolbox (version 4.8)[11] was used, allowing variant rigidity penalties to properly model the different deformation properties of solid and soft tissues. Applying the deformation to the MRI yielded a registered MRI (rMRI). The performance of each registration was verified by manual inspection.

## 2.C Synthetic CT generation

Synthetic CT images were generated from the rMRI using the TFE algorithm, which was provided through the MRI Planner v2.3 software (Spectronic Medical AB, Helsingborg, Sweden). The output of the MRI Planner software constitutes both an sCT provided as standard DICOM files, and also a full set of automatically generated organ contours provided as a DICOM RT-STRUCT file. MRI Planner is a commercially available CE marked software that can be installed on a computer at the hospital. Processing time to generate an sCT with organ contours is 4–6 minutes

MRI Planner first performs a DICOM tag analysis to verify that the incoming MRI is compatible with MRI Planner and that it is in conformance with the acquisition protocol specified by the user. The TFE algorithm then calculates a CT representation for the incoming MRI by first estimating the spatially variant coefficients of an affine transfer function and then applying this transfer function to the MRI. The coefficients of the transfer function are generated using a spe-

cialized structure of deep convolutional neural networks. The networks are trained using a multi center database of paired MR and CT images acquired using a similar protocol as is used in the present study, along with a large set of expert OAR contours. Since the networks are trained with a very high degree of data augmentation, they are robust to a large variety of MRI scanners and acquisition parameters. The main requirement of the incoming MRI is therefore that its acquisition contrast largely resembles that of the training MRIs. In addition, since the size of the final sCT is equal to that of the incoming MRI, certain physical requirements also apply, such as having a large enough FOV to capture the entire volume of interest and having a sufficient resolution to allow dose calculations.

The utilized neural network structure consists of multiple high-resolution 3D networks, each consisting of multiple convolutional layers arranged in a specialized network topology. The networks are designed such that they have a large perceptible field of view, providing a high degree of context awareness and inference robustness throughout all parts of the image. In addition, the networks are provided with multiple residual connections, in order to allow data propagation when reduced network complexity is beneficial.

An MR image is resampled to a standard resolution and is provided as the input to the network structure. The final output is a multi-channel 3D volume, consisting of both the spatially variant coefficients of the transfer function along with a label classification describing which OAR structure each image voxel belongs to. The spatial coefficients are provided to the transfer function, which is then applied to the original MRI to generate the sCT. The generated sCT thereby preserves the original resolution of the MRI, without any loss of detail.

Once the TFE algorithm is finished the MRI Planner software invokes a separate quality assurance algorithm (QAA) to perform a secondary verification of the generated sCT. The QAA analyzes the histogram of the generated sCT and compares it to a statistical HU distribution derived from a large database of pelvic CT images. The purpose of the QAA is to provide an additional security measure to assure that the generated sCT is of high quality. The presence of anomalies is extremely unlikely, unless there are severe problems with the acquired MR data. No such anomalies were seen in the present study.

Upon installation, the TFE algorithm is ready to use, with no requirement to acquire any additional training data. It should be noted that the TFE algorithm is configured to not propagate gas cavities in the rectum from the MRI to the sCT. Due to the volatile nature of rectal cavities and the high probability of such cavities not appearing at the same location during therapy, the content of the rectum is instead configured as water equivalent in the sCT.

## 2.D Treatment planning

For each patient, a 5-field 6 MV intensity modulated radiation therapy (IMRT) plan was generated using matRad [12]

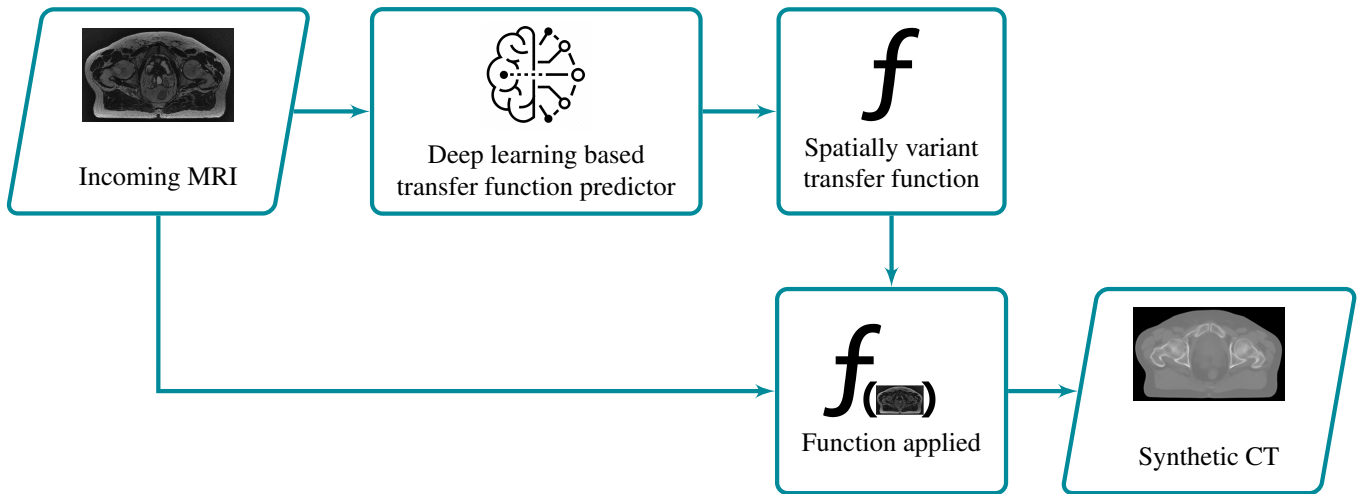


Figure 1. Schematic drawing of the transfer function estimation (TFE) algorithm

Table 2. Optimization objectives for the inverse treatment planning

Structure/ Objective	Dose level [Gy]	Volume [%]	Penalty
<b>Prostate</b>			
Squared deviation	78.0	N/A	800
Min DVH	74.1	95.0	1000
<b>Bladder</b>			
Max DVH	70.0	15.0	800
Max DVH	59.0	35.0	500
Max DVH	51.0	45.0	300
<b>Colon</b>			
Max DVH	70.0	15.0	800
Max DVH	59.0	35.0	500
Max DVH	51.0	45.0	300
<b>Femoral heads</b>			
Squared overdosing	55.0	N/A	600

(version 2.2). Each treatment plan was created for the CT and recalculated for the sCT using the same weight factors. The pencil beam algorithm implemented in matRad was used for dose calculations with an in-plane resolution of  $2.5 \times 2.5$  mm, while the resolution in the slice direction was governed by slice thickness in the CT. Prior to treatment planning all CTs were converted to the same CT-calibration curve on which MRI Planner generates sCTs.

The automatically generated structures provided from MRI Planner were used in the treatment planning optimization and dose evaluation. The objectives defined in table 2 were applied in the optimization.

## 2.E Patient positioning verification

Patient positioning verification was evaluated for ten prostate cancer patients using a triplet of images per case; CBCT, CT and sCT. The CBCT was used as the reference image and

both CT and sCT were rigidly registered to the reference using the Elastix toolbox [11] (version 4.8). The registration was focused solely on bone structures in the images. This was achieved by applying a thresholding on all images with a lower cutoff at 200 HU. The registration was initialized by aligning the centre of masses of the thresholded images. Since the CT and sCT were already in the same frame of reference (through the use of the rMR for sCT generation), no additional step was required in order to bring the images to a common reference point. Evaluation was then performed based on the six dimensional transformation matrix generated by each registration.

## 2.F Evaluation

For each patient, mean HUs and mean absolute errors (MAE)[13, 14] of HUs were compared between sCT and CT, with respect to bone structures, soft-tissue and full body contour. MAE is calculated for all voxels,  $N$ , within the respective segments by

$$MAE = \frac{1}{N} \sum_{i=1}^N |sCT_i - CT_i| \quad (1)$$

Bone structure segments were generated for sCT and CT separately by thresholding the respective images at 100 HU, followed by a morphological hole filling to also include the softer bone and the bone marrow contained inside the compact bone. Soft tissue segments were generated by thresholding the sCTs and CTs at -100 HU and subtracting the previously generated bone structures. Body contour segments were similarly generated by thresholding the sCTs and CTs at -650 HU, followed by a morphological hole-filling to also include gas cavities inside the body.

The average absorbed dose differences to the prostate and organs at risk (bladder, colon and femoral heads) were compared between sCT and CT. Additionally, a set of dose volume constraints from the HYPO-RT-PC study protocol[15]

**Table 3.** Mean absolute HU, mean difference and mean absolute error (MAE) between sCT and CT for different tissue segments. Uncertainty given as the standard deviation between cases.

Segment	sCT [HU]	CT [HU]	$\Delta$ HU	MAE [HU]
Body	-17.2 (11.4)	-9.5 (13.7)	-7.7 (7.3)	39.6 (6.7)
Soft	-21.4 (7.0)	-12.2 (7.1)	-9.2 (4.8)	24.2 (3.0)
Bone	268.3 (24.8)	286.5 (40.1)	-18.2 (24.5)	95.0 (12.8)

(minimum dose to target, volume of target covered by the 95% isodose, dose encompassing 99% of the target volume, volume of colon receiving more than 65%, 75% and 90% of the prescribed dose, maximum dose to femoral heads and maximum dose to body) were compared accordingly. 3D gamma evaluation [16] was computed using pyMedPhys (version 0.8.4) where the CT-based dose distribution was used as the reference and consequently the sCT-based dose distribution as evaluation. The evaluation criterion was 2%/2mm with a lower dose cut off at 11.7 Gy (15% of the prescribed dose).

Finally, patient positioning verification was evaluated. For each patient the positioning difference between CT and sCT was measured by computing the difference between registrations to CBCT. The average difference and standard deviation was calculated independently for each degree of freedom, including both translation and rotation.

### 3. Results

Mean HU whole body difference between all sCT and CT was  $-7.7 \pm 7.3$  HU. Corresponding MAE was  $39.6 \pm 6.7$  HU. A complete list of HU comparison parameters are found in table 3.

The mean target dose difference was found to be  $-0.02 \pm 0.23$  Gy. A comprehensive list of differences for all evaluated DVH parameters is given in (Table 4). Moreover the distribution of differences on mean doses for all evaluated structures is displayed in fig. 2. The average gamma passing rate was 99.94% with a range of [99.50, 100.00] %.

The difference in sCT–CBCT to CT–CBCT positioning was  $0.02 \pm 0.27$  mm and  $0.05 \pm 0.29$  ° for translations and rotations, respectively. A full break down of results per degree of freedom are found in table 5.

All uncertainties above are given as one standard deviation for the population.

### 4. Discussion

Using a single standard MR image series of the male pelvic region, the MRI Planner software uses the TFE algorithm to generate sCT images for absorbed dose calculations and patient positioning in prostate radiotherapy. In the present study MR-images were acquired using a T2 weighted sequence with four separate MRI scanners, at either 1.5T or 3T.

Both the treatment planning and patient positioning study of this work shows results that are highly similar between

**Table 4.** Average dose deviation between sCT and CT. Relative differences (left column) expressed in percentage of prescribed dose (mean, maximum, minimum, and D99%) or local volume percentage difference (V90%, V75%, and V65%) and absolute differences (right column) absolute change (in Gy) or volume percentage point difference.

	Relative deviation	Absolute deviation
<b>Body</b>		
Max	0.12 (0.48)	0.09 (0.37)
<b>Target</b>		
Mean	-0.02 (0.30)	-0.02 (0.23)
Min	-0.24 (0.38)	-0.18 (0.30)
D99%	-0.20 (0.36)	-0.16 (0.28)
V95%	-0.01 (0.03)	-0.01 (0.03)
<b>Bladder</b>		
Mean	0.00 (0.06)	0.00 (0.05)
<b>Colon</b>		
Mean	-0.03 (0.13)	-0.02 (0.10)
V90%	-1.72 (5.14)	-0.07 (0.21)
V75%	-0.72 (1.96)	-0.08 (0.25)
V65%	-0.23 (1.30)	-0.03 (0.20)
<b>Femoral head left</b>		
Mean	0.00 (0.04)	0.00 (0.03)
Max	-0.01 (0.20)	-0.03 (0.15)
<b>Femoral head right</b>		
Mean	-0.01 (0.04)	0.00 (0.03)
Max	-0.03 (0.20)	-0.02 (0.15)

sCT and CT. Thus, the results show that prostate MRI only radiotherapy planning is clinically feasible using the TFE and that the TFE is robust to images acquired using a variety of MRI scanners.

When comparing an MRI based synthetic CT to a conventional CT, there are two interacting processes that may both affect the results. First is the performance of the algorithm by which the sCT is generated and second is the geometric agreement between the MRI and the CT. The second of these processes may result from inaccuracies in patient repositioning between image sessions, differences in bladder and/or rectal filling between images, or due to geometric distortions in the MRI. Thus, in order to properly evaluate the algorithm alone, these two processes need to be discriminated, which is

**Table 5.** Average difference in sCT–CBCT to CT–CBCT positioning per degree of freedom. All uncertainties are given as one standard deviation.

Dimension	Translation [mm]	Rotation [°]
x	-0.13 (0.26)	-0.04 (0.10)
y	0.04 (0.29)	-0.05 (0.07)
z	0.15 (0.15)	0.24 (0.43)

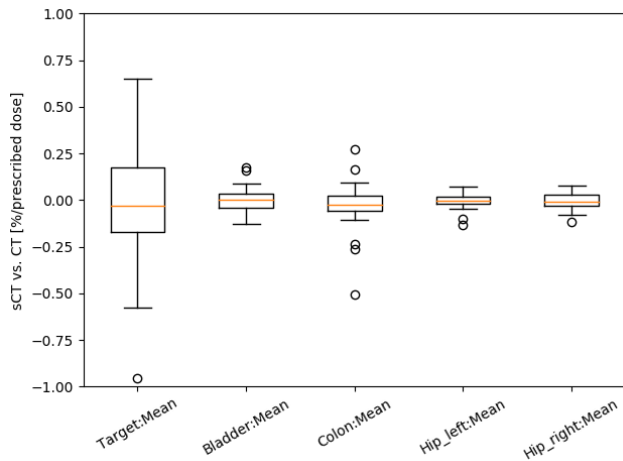


**Figure 2.** Boxplot of per structure relative dose difference between sCT and CT normalized to prescribed dose. The bars represent the median, boxes cover the third to first interquartile range (IQR) while the whiskers extends to data points at 1.5IQR. Outliers are marked as circles.

achieved in this work by the introduction of the rMR.

In an MRI only workflow it is important to verify the geometric integrity of the MRI, since geometric distortions will directly propagate to the sCT and may thereby have a dosimetric impact. However, several studies have shown that the effects of such distortions are generally negligible[17, 10], provided that high image acquisition bandwidth is used and that the built-in distortion correction provided with the MRI scanner is activated. In the present study, the quality assurance functionality of the MRI Planner software was used to verify that all images were conforming with such image acquisition protocol.

As a routine measure, phantom measurements may be performed by regular interval to assure that the MRI scanner is operating correctly with regard to geometric integrity. Of particular importance is to use a phantom solution that can verify the geometry of the full field of view of the scanner, as all aspects of the image is of importance in an MRI only setting. For this purpose a solution such as the Spectronic Medical GRADE phantom and software can be used for such QA procedures[18].

A high level of accuracy is required in all steps of the radiotherapy process in order to deliver treatments that result in high tumor control probability and minimal risk to normal tissue. The literature suggests that an overall dose accuracy of 2.5-3.5% is needed to meet such clinical requirements[19, 20, 21]. Given that the  $\Delta\bar{D}_{\text{Prostate}}$  between sCT and CT is in the range of -0.96% to 0.65% for every evaluated case, it appears that the uncertainty contribution added by the TFE is negligible in this context.

## 5. Conclusions

The TFE generates sCT images that enables an accurate MRI only workflow in prostate radiotherapy planning. Any uncertainties associated with the TFE, regarding dose accuracy or patient positioning, appear negligible and the results of this work suggest performance well within published clinical requirements.

## Acknowledgments

This work was supported the Swedish Agency for Innovation Systems (VINNOVA).

We would like to thank Skåne University Hospital, Umeå University Hospital, Sahlgrenska University Hospital and Karolinska University Hospital for the image material used in this work[10].

The authors declare that they are employed by Spectronic Medical AB.

## References

- [1] C. Rasch, P. Remeijer, P. C. Koper, G. J. Meijer, J. C. Stroom, M. van Herk, and J. V. Lebesque. Comparison of prostate cancer treatment in two institutions: a quality control study. *Int. J. Radiat. Oncol. Biol. Phys.*, 45(4):1055–1062, 1999.
- [2] M. Debois, R. Oyen, F. Maes, G. Verswijvel, G. Gatti, H. Bosmans, M. Feron, E. Bellon, G. Kutcher, H. Van Poppel, and L. Vanuytsel. The contribution of magnetic resonance imaging to the three-dimensional treatment planning of localized prostate cancer. *Int. J. Radiat. Oncol. Biol. Phys.*, 45(4):857–865, 1999.
- [3] Y. K. Lee, M. Bollet, G. Charles-Edwards, M. A. Flower, M. O. Leach, H. McNair, E. Moore, C. Rowbottom, and S. Webb. Radiotherapy treatment planning of prostate cancer using magnetic resonance imaging alone. *Radiother Oncol*, 66(2):203–216, 2003.
- [4] J. H. Jonsson, A. Johansson, K. Soderstrom, T. Asklund, and T. Nyholm. Treatment planning of intracranial targets on MRI derived substitute CT data. *Radiother Oncol*, 108(1):118–122, 2013.
- [5] L. Liu, Y. Cao, J. A. Fessler, S. Jolly, and J. M. Balter. A female pelvic bone shape model for air/bone separation in support of synthetic CT generation for radiation therapy. *Phys Med Biol*, 61(1):169–182, 2016.
- [6] L. Liu, S. Jolly, Y. Cao, K. Vineberg, J. A. Fessler, and J. M. Balter. Female pelvic synthetic CT generation based on joint intensity and shape analysis. *Phys Med Biol*, 62(8):2935–2949, 2017.
- [7] J. A. Dowling, J. Lambert, J. Parker, O. Salvado, J. Frripp, A. Capp, C. Wratten, J. W. Denham, and P. B. Greer. An atlas-based electron density mapping method for magnetic resonance imaging (MRI)-alone treatment planning

- and adaptive MRI-based prostate radiation therapy. *Int. J. Radiat. Oncol. Biol. Phys.*, 83(1):5–11, 2012.
- [8] C. Siversson, F. Nordstrom, T. Nilsson, T. Nyholm, J. Jonsson, A. Gunnlaugsson, and L. E. Olsson. Technical Note: MRI only prostate radiotherapy planning using the statistical decomposition algorithm. *Med Phys*, 42(10):6090–6097, 2015.
- [9] X. Han. MR-based synthetic CT generation using a deep convolutional neural network method. *Med Phys*, 44(4):1408–1419, 2017.
- [10] E. Persson, C. Gustafsson, F. Nordström, M. Sohlén, A. Gunnlaugsson, K. Petruson, M. Rintelä, K. Hed, L. Blomqvist, B. Zackrisson, T. Nyholm, L.E. Olsson, C. Siversson, and J. Jonsson. Mr-opera : A multicenter/multivendor validation of magnetic resonance imaging-only prostate treatment planning using synthetic computed tomography images. 99(3):692–700, 2017.
- [11] S. Klein, M. Staring, K. Murphy, M. A. Viergever, and J. P. Pluim. elastix: a toolbox for intensity-based medical image registration. *IEEE Trans Med Imaging*, 29(1):196–205, 2010.
- [12] Hans-Peter Wieser, Eduardo Cisternas, Niklas Wahl, Silke Ulrich, Alexander Stadler, Henning Mescher, Lucas-Raphael Müller, Thomas Klinge, Hubert Gabrys, Lucas Burigo, et al. Development of the open-source dose calculation and optimization toolkit matrad. *Medical Physics*, 44(6):2556–2568, 2017.
- [13] A. Johansson, M. Karlsson, J. Yu, T. Asklund, and T. Nyholm. Voxel-wise uncertainty in CT substitute derived from MRI. *Med Phys*, 39(6):3283–3290, 2012.
- [14] C. M. Rank, C. Tremmel, N. Hunemohr, A. M. Nagel, O. Jakel, and S. Greilich. MRI-based treatment plan simulation and adaptation for ion radiotherapy using a classification-based approach. *Radiat Oncol*, 8:51, 2013.
- [15] A. Widmark, A. Gunnlaugsson, L. Beckman, C. Thellenberg-Karlsson, M. Hoyer, M. Lagerlund, J. Kindblom, C. Ginman, B. Johansson, K. Bjornlinder, M. Seke, M. Agrup, P. Fransson, B. Tavelin, D. Norman, B. Zackrisson, H. Anderson, E. Kjellen, L. Franzen, and P. Nilsson. Ultra-hypofractionated versus conventionally fractionated radiotherapy for prostate cancer: 5-year outcomes of the HYPO-RT-PC randomised, non-inferiority, phase 3 trial. *Lancet*, 394(10196):385–395, 2019.
- [16] D. A. Low, W. B. Harms, S. Mutic, and J. A. Purdy. A technique for the quantitative evaluation of dose distributions. *Med Phys*, 25(5):656–661, 1998.
- [17] Christian Jamtheim Gustafsson, Fredrik Nordström, E Persson, Johan Brynolfsson, and Lars Olsson. Assessment of dosimetric impact of system specific geometric distortion in an mri only based radiotherapy workflow for prostate. *Physics in Medicine and Biology*, 62:2976–2989, 04 2017.
- [18] Spectronic Medical AB. Geometry distortion assessment using grade. <http://www.spectronic.se/grade/>. Accessed: 2019-12-20.
- [19] A. Brahme. Dosimetric precision requirements in radiation therapy. *Acta Radiol Oncol*, 23(5):379–391, 1984.
- [20] M. Goitein. Nonstandard deviations. *Med Phys*, 10(5):709–711, 1983.
- [21] B. J. Mijnheer, J. J. Battermann, and A. Wambersie. What degree of accuracy is required and can be achieved in photon and neutron therapy? *Radiother Oncol*, 8(3):237–252, 1987.